Quality and Consistency of the NASA Ocean Color Data Record

Bryan A. Franz[1], Sean W. Bailey[1,2], Gerhard Meister[1], and P. Jeremy Werdell[1]

[1]NASA Goddard Space Flight Center, Greenbelt, Maryland, USA
[2]Futuretech Corporation, Greenbelt, Maryland, USA

ABSTRACT

The NASA Ocean Biology Processing Group (OBPG) recently reprocessed the multi-mission ocean color time-series from SeaWiFS, MODIS-Aqua, and MODIS-Terra using common algorithms and improved instrument calibration knowledge. Here we present an analysis of the quality and consistency of the resulting ocean color retrievals, including spectral water-leaving reflectance, chlorophyll *a* concentration, and diffuse attenuation. Statistical analysis of satellite retrievals relative to in situ measurements will be presented for each sensor, as well as an assessment of consistency in the global time-series for the overlapping periods of the missions. Results will show that the satellite retrievals are in good agreement with in situ measurements, and that the sensor ocean color data records are highly consistent over the common mission lifespan for the global deep oceans, but with degraded agreement in higher productivity, higher complexity coastal regions.

INTRODUCTION

The science of ocean color involves the measurement of the spectral distribution of reflected visible solar radiation upwelling from below the ocean surface. Variations in this water-leaving "remote sensing" reflectance distribution, $R_{rs}(\lambda)$, the ratio of radiance emerging from beneath the ocean surface to the solar irradiance reaching the ocean surface, are governed by the biological and chemical constituents of the upper ocean mixed layer through their influence on the absorption and scattering properties (Morel and Prieur 1977). In the deep oceans, away from terrestrial influences, the primary driver for variations in ocean color is the concentration of the phytoplankton pigment chlorophyll-*a* (Chl *a)*. Bio-optical algorithms have been developed that relate measurements of $R_{rs}(\lambda)$ to Chl *a*, thus providing a mechanism for making remote estimates of Chl *a* concentrations that can be related to phytoplankton biomass, a significant component of marine carbon stocks and a critical element of the global carbon cycle (Chisholm 2000). Another geophysical parameter that is derived from $R_{rs}(\lambda)$ is the diffuse attenuation at 490 nm (Kd490), which is a measure of light penetration depth that impacts phytoplankton growth rates and is a required input for modeling of marine net primary productivity (Behrenfeld et al. 2006).

The measurement of $R_{rs}(\lambda)$ from spaceborne instruments is challenging because the water-leaving signal is only a small fraction of the total signal reflected by the earth into the sensor field of view. Approximately 90% of the visible radiation observed by earth-viewing satellite sensors is sunlight reflected by air molecules and aerosols in the atmosphere. Other contributions are associated with light reflected by the ocean surface that does not interact with the water column and thus carries no information on the concentrations of water column constituents. The removal of these atmospheric and surface contributions is generally referred to as atmospheric correction. Since the water-leaving contribution is such a small part of the total observed radiance, $R_{rs}(\lambda)$ retrievals from spaceborne sensors are highly sensitive to errors or inconsistencies in the atmospheric correction algorithm and the sensor calibration. In effect, a 1% error in the atmospheric correction or the sensor calibration

B.A. Franz, S.W. Bailey, G. Meister, and P.J. Werdell, "Consistency of the NASA Ocean Color Data Record," *Proc. Ocean Optics 2012*, Glasgow, Scotland, 8-12 October 2012.

translates to a 10% difference in the water-leaving reflectance, which can result in even larger differences in derived geophysical parameters.

A primary goal of the OBPG is to produce a Climate Data Record (CDR) for Ocean Color: a timeseries of measurements of sufficient length, consistency, and continuity to determine climate variability and change (National Research Council, 2004). Given the relatively short duration of satellite missions, this goal requires the production of a consistent timeseries across multiple ocean color missions (Siegel and Franz 2010). The OBPG currently maintains the ocean color data records from a variety of past and present satellite sensors, including Sea-Viewing Wide-field-of-view Sensor (SeaWiFS, 1997-2010, McClain et al. 1998) and Moderate Resolution Imaging Spectroradiometer (MODIS, Esaias et al. 1998) on both Terra (MODIST, 1999-present) and Aqua (MODISA, 2002-present). Recently, the OBPG completed a comprehensive reprocessing of these ocean color missions with the goal of producing a continuous, consistent, and accurate ocean color record spanning their combined lifespans. Here, we describe the processing approach and assess the results of SeaWiFS, MODIST, and MODISA ocean color reprocessing 2010.0 (R2010.0), and the subsequently updated MODISA reprocessing 2012.0 (R2012.0).

APPROACH

The OBPG relies on a three-part approach to minimize error in $R_{rs}(\lambda)$ retrievals from multiple spaceborne sensors.

1. Focus on the instrument calibration (e.g., prelaunch characterization, periodic lunar and/or solar observations), to maximize temporal and cross-scan stability within each mission.

2. Apply a common atmospheric correction approach to all sensors, to minimize inconsistencies in the retrieval process.

3. Apply vicarious calibration to a common ground source, to minimize bias due to residual atmospheric correction or absolute calibration errors, and maximize spectral consistency.

Instrument Calibration

The SeaWiFS instrument calibration is detailed in Eplee et al. (2012). The instrument design employs a rotating telescope to scan the earth as the satellite progresses, thus ensuring a constant angle of incidence relative to the primary mirror and thereby minimizing differences in radiometric response with scan angle. Monthly observations of the moon are therefore sufficient to track temporal degradation in radiometric response, which is largest in the near infrared (NIR) wavelengths where changes on the order of 20% were observed over the 13-year mission lifespan. The temporal changes are well characterized using the lunar calibration, with uncertainty on the order of a few tenths percent.

The MODIS instruments are more challenging to calibrate, as they employ a large rotating mirror to scan the earth, and the reflectivity of the mirror varies with angle of incidence giving rise to a significant variation in response versus scan angle (RVS). The MODIS Calibration Support Team (MCST) provides the primary calibration for the two MODIS instruments (Xiong et al. 2003). The MCST calibration approach historically relies on frequent observations of the Sun to track the temporal degradation at one scan angle (near end of scan), and monthly observations of the Moon to track

changes at another scan angle (near the beginning of the scan). With these two measurements, MCST can correct for temporal changes in RVS by assuming a linear relationship in RVS changes across all scan angles. The OBPG has found this assumption of linearity to be insufficiently accurate for ocean color retrievals (Meister et al. 2012). For the R2010.0 ocean color reprocessing of MODISA, the OBPG utilized a cross calibration technique relative to SeaWiFS to correct for nonlinear changes in the shape of the RVS, but only for the blue bands at 412 and 443 nm where degradation in radiometric response is largest (of order 50%). Recently, MCST acknowledged the limitations of the standard calibration approach and developed an alternative calibration for the 412 and 443-nm spectral bands based on desert observations (unpublished to date), which largely reproduces the SeaWiFS-based OBPG calibration corrections of R2010.0, but with the advantage of independence from the now defunct SeaWiFS mission. This latest MCST calibration was applied in the Collection 6 (C6) reprocessing of MODISA land and atmospheres products, and was adopted as the baseline for the OBPG for ocean color reprocessing. The MCST C6 calibration, however, augmented with additional statistical corrections to minimize detector-to-detector, mirror-side to mirror-side, and residual RVS artifacts (Meister et al. 2013). This revised instrument calibration was applied in MODISA ocean color reprocessing R2012.0.

Establishing sufficient calibration stability in the MODIST data record is an even greater challenge, due to issues with the primary mirror and limitations of the on-board calibration system as detailed in Franz et al. (2008). To make the instrument useful for ocean color, the OBPG augmented the standard MCST Collection 5 (C5) calibration with temporally varying corrections to the RVS and cross-scan polarization sensitivity (Meister et al. 2005) in all visible spectral bands (relative to the prelaunch characterization and MCST temporal calibration). These corrections were derived with a cross-calibration approach using SeaWiFS as the calibration source (Kwiatkowska et al. 2008), and applied in the R2010.0 MODIST ocean color reprocessing. As such, the MODIST ocean color timeseries from R2010.0 cannot be considered a fully independent CDR. MCST has now developed a desert-based calibration for MODIST (like that of MODISA) in preparation for MODIST C6 reprocessing, which will likely be adopted for the next MODIST ocean color reprocessing (R2012.0).

Algorithms

To minimize inconsistency in the atmospheric correction between the sensors, the OBPG utilizes sensor-independent, common processing software and algorithms in the conversion of Level-1B calibrated TOA radiances to Level-2 $R_{rs}(\lambda)$ and derived geophysical products and Level-3 global composites (OBPG 2012a). The standard atmospheric correction approach for all sensors is that of Gordon and Wang (1994), with a number of significant updates detailed in Table 1.

While the atmospheric correction approach is identical between the sensors, differences in spectral band centers and spectral band response must be considered. This is done through sensor-specific atmospheric tables that account for the full spectral bandpass of each instrument (Gordon 1995). To ensure consistency, all bandpass-specific tables were regenerated for R2010.0 using common sources and methods, including band-averaged Rayleigh optical thicknesses and depolarization factors (derived using the model of Bodaine et al. 1999 and assuming standard pressure of 1013.25mb, temperature of 288.15K, and CO2 concentration of 360ppm), band-averaged ozone and NO_2 absorption cross-sections, and band-averaged mean solar irradiances using the source spectrum of Thuillier et al. (2003). The updated Rayleigh optical thicknesses and depolarization factors were then used in new

vector radiative transfer simulations (Ahmad et al. 2010) to derive the sensor-specific Rayleigh and aerosol reflectance and diffuse transmittance tables that are used in the atmospheric correction process.

Atmospheric Correction Algorithm Change	References and Details
corrections for broad spectral bands and out-of-band response	Gordon 1995, Wang et al. 2001 (updated to use model of Werdell et al. 2007), Franz et al. 2003.
corrections for polarization sensitivity	Gordon et al. 1995, Meister et al. 2005.
updated Rayleigh atmospheric scattering tables	Wang 2002, updated using radiative transfer simulations of Ahmad et al. 2010.
updated aerosol models and aerosol selection scheme	Ahmad et al. 2010.
correction for non-zero water-leaving radiances in the near infrared	Bailey et al. 2010 and references therein.
diffuse transmittance effects	Wang 1999, updated using radiative transfer simulations of Ahmad et al. 2010.
gaseous transmittance effects	added NO2 absorption, Ahmad et al. 2007.
updated sun glint correction	Wang and Bailey 2001.
whitecap contributions	Frouin et al. 1997, Moore et al. 2000, Stramska et al. 2003., http://oceancolor.gsfc.nasa.gov/REPROCESSING/R2009/whitecap/
bidirectional reflectance effects	added Morel et al. 2002, Gordon 2005, Wang 2006.

Table 1: *Atmospheric correction algorithm changes relative to Gordon and Wang (1994).*

Since every step in the atmospheric correction effectively accounts for the full spectral response in each sensor band, the resulting water-leaving radiance retrievals are based on the full spectral bandpass. To remove the effect of sensor-specific out-of-band response from the $R_{rs}(\lambda)$, the full-bandpass water-leaving radiances were adjusted to that for square 11-nm bandpasses (Wang et al. 2001) located at the nominal band centers (Table 2) using the model of Werdell et al. 2007. The fully normalized, nominal-band water-leaving radiances were then converted to $R_{rs}(\lambda)$ using nominal-center-band-averaged mean solar irradiances (Franz et al. 2003).

The retrieved $R_{rs}(\lambda)$ at each visible sensor wavelength provide the basis for many derived geophysical product algorithms. The standard algorithms for Chlorophyll-*a* (Chl *a*, OBPG 2012b) and diffuse attenuation at 490 nm (Kd490, OBPG 2012c) are empirical $R_{rs}(\lambda)$ band ratio algorithms, where the coefficients were tuned using the NASA bio-Optical Marine dataset (NOMAD, Werdell and Bailey 2005). NOMAD provides a dataset of in situ biogeochemical measurements with coincident in situ R_{rs} measurements at various wavelengths. To account for differences in the nominal center wavelengths of each sensor, the tuning dataset was restricted to measurements of in situ R_{rs} that are at or near the nominal satellite sensor wavelengths of Table 2. Thus, while the Chl *a* and Kd490 algorithms are very similar for each instrument, the algorithm coefficients differ between SeaWiFS and the two MODIS sensors to account for differences in nominal band wavelengths.

Sensor	Nominal Center Wavelengths (nm)
SeaWiFS	412,443,490,510,555,670,765,865
MODISA & MODIST	412,443,469,488,531,547,555,645,667,678,748,859,869,1240,1640,2130

visible ocean color bands, primary atmospheric correction bands, land bands

Table 2: *SeaWiFS and MODIS Nominal Center Wavelengths*

Vicarious Calibration

Given the stringent accuracy requirements of satellite ocean color retrievals for both the instrument calibration and the atmospheric correction algorithm, the OBPG employs an additional calibration wherein the TOA radiance calibration is adjusted to force average agreement of the $R_{rs}(\lambda)$ retrievals to

ground-based measurements. This temporaly-independent but wavelength-specific vicarious calibration minimizes residual bias and enhances spectral consistency of the sensor + algorithm system under idealized conditions (Franz et al. 2007). All ocean color missions launched after 1996 and processed by the OBPG have utilized the Marine Optical Buoy (MOBY) near Lanai Hawaii as a common vicarious calibration source (Clark et al. 1997), thus minimizing relative bias in $R_{rs}(\lambda)$ between missions.

RESULTS AND DISCUSSION

Comparison with Field Data

The primary mechanism for assessing the quality of the satellite ocean color retrievals is through comparison with in situ measurements. Match-up in satellite retrievals of $R_{rs}(\lambda)$, Chl *a*, and Kd490 with in situ measurements was performed using the standard criteria detailed in Bailey and Werdell (2006), using all available in situ data from the SeaWiFS Bio-optical Archive and Storage System (SeaBASS, Werdell et al. 2003) as well as the AERONET-OC database, a subset of sensors within the Aerosol Robotic Network that are also configured to collect above water ocean color radiometry (Zibbordi et al. 2006). Figure 1 shows the geographic distribution of in situ match-ups for the SeaWiFS sensor, Figure 2 shows the associated comparisons of SeaWiFS retrievals with in situ measurements of Chl *a*, Kd490, and $R_{rs}(\lambda)$ at two critical ocean color bands, and Table 3 provides a statistical analysis of the satellite to in situ match-ups for $R_{rs}(\lambda)$ at all visible ocean color bands for SeaWiFS, MODISA, and MODIST. Results are shown separately for AERONET-OC and SeaBASS match-ups, thus providing two independent assessments of satellite $R_{rs}(\lambda)$ retrieval performance relative to ground truth. Table 2 also shows statistical analyses for all deep-water SeaBASS measurements (depth greater than 1000 meters), to show how the retrieval algorithms perform in the open-ocean environment, away from the complexities of coastal variability and terrestrial influences. Table 4 provides a similar statistical analysis for SeaBASS match-ups (global and deep-water) of Chl *a* and Kd490. The analysis includes the R^2 coefficient to demonstrate the level of correlation, the median ratio of satellite to in situ measurements as an indicator of bias, and the mean absolute percent difference (APD) as an indicator of uncertainty.

In general, the results of Figure 2 and Tables 3 and 4 demonstrate a high degree of correlation between satellite retrievals and in situ measurements of $R_{rs}(\lambda)$. When match-ups are restricted to deep water, retrievals for all three sensors show minimal bias (within a few percent) at all wavelengths except in the red (667-670 nm), where signals in relatively clear ocean waters are very low and instrumental noise becomes more significant. Deep-water $R_{rs}(\lambda)$ uncertainties, as measured by mean APD, range from 8% in the green to 16% in the blue. As expected, bias and uncertainty increases when all SeaBASS match-ups are considered, especially in the 412-nm wavelength.

The additional SeaBASS match-ups in complex coastal waters contribute cases of high 412-nm absorption from elevated concentrations of dissolved organic matter and chlorophyll, which leads to low signal at 412-nm and thus greater impact of instrumental noise and calibration error in that band. This is compounded by greater uncertainties in the atmospheric correction algorithm due to the presence of absorbing aerosols (dust, smoke, soot) from terrestrial sources and human activity, and turbid or highly productive waters that reflect significantly in the NIR. Non-zero water-leaving reflectance in the NIR confounds the aerosol determination in the atmospheric correction algorithm, so the effect is estimated and removed using a bio-optical modeling approach (Bailey et al. 2010) that

likely contributes additional uncertainty. With the observing capabilities of SeaWiFS and MODIS alone, absorbing aerosols are not easily discernable from non-absorbing aerosols, so the effect of absorbing aerosols is not identified or removed by the current atmospheric correction algorithm, leading to increased negative bias in the $R_{rs}(\lambda)$ retrievals, especially in the shortest wavelengths. The AERONET-OC stations are all located on land or near-shore platforms, and thus bias and uncertainty of the satellite retrievals relative to AERONET-OC are similar or further increased relative to the global SeaBASS match-up results. Note that R^2 correlation does not necessarily degrade with increasing water complexity, since the increased uncertainty is balanced by increased dynamic range that enhances the robustness of that statistic. It should also be considered that the validity of the satellite to in situ match-up analysis as a measure of satellite retrieval error or uncertainty is degraded in coastal waters, due to real spatial variability at the sub-pixel level (within the approximately 1x1 km^2 satellite footprint), and real temporal variability. In inhomogeneous waters, both the satellite retrieval and the in situ measurement could be perfectly correct, but the two may differ significantly if the in situ measurement was not made in a location that is representative of the mean within the satellite pixel footprint.

As for $R_{rs}(\lambda)$, the Chl *a* match-up comparisons in Table 4 shows that bias, as determined by the median ratio of satellite to in situ measurements, increases from 0-5% in deep water to 1-15% for the global SeaBASS analysis, and uncertainty increases from 25-30% in deep water to 35-40% for all SeaBASS measurements. The increased uncertainty with increased complexity is not as significant for Chl *a* as for some of the R_{rs} measurements, likely because the band-ratio algorithm used to derive Chl *a* from $R_{rs}(\lambda)$ mitigates the impact of spectrally correlated atmospheric correction biases in the $R_{rs}(\lambda)$ retrievals. The Kd490 results show median bias within 10% and mean APD within 20% for both deep-water and global SeaBASS cases for the three satellite missions.

An important result of the analyses in Tables 3 and 4 is that all three sensors are generally showing very similar performance relative to the in situ measurements. This is further illustrated in Table 5, where the same statistical analyses are performed between satellite retrievals (SeaWiFS versus MODISA and SeaWiFS versus MODIST) at the common in situ match-up locations. Correlation coefficients range from 0.8 to 0.95 in the blue to green $R_{rs}(\lambda)$ retrievals between the satellite pairs, with mean bias within 10% and mean APD within 15% (slightly higher in the longest and shortest bands). Similarly, the Chl *a* and Kd490 retrievals agree well between the satellite sensor pairs, with R^2 of 0.9 or better, mean bias within 5%, and mean APD of 13% and 8% for Chl *a* and Kd490, respectively. The fact that the satellite to satellite mean APD is roughly one half to one third the satellite to in situ APD suggests that some significant fraction of the variability in the satellite to in situ match-ups is due to systematic but consistent error in the satellite retrieval algorithm, noise in the in situ data, or real variability at the sub-pixel scale.

Comparison of Global Trends

The preceding analysis looked at uncertainty and consistency in Level-2 ocean color retrievals, but for earth system research and global change studies the primary data products of interest are the Level-3 global binned composites (e.g., data binned into daily, 8-day, or monthly means on a global grid) from which regional to global-scale trends can be derived. A primary concern in trend analysis is temporal stability of the time-series, to ensure that systematic errors such as uncorrected degradation in instrument radiometric response are not misinterpreted as geophysical changes. A useful measure of

temporal stability is the assessment of consistency in the ocean color timeseries from different sensors over the common mission lifespan, as provided in Figures 3 and 4 and Tables 6 and 7.

The comparative trends shown in Figures 3 and 4 were derived from monthly Level-3 binned R_{rs} and Chl *a* products at 9.2-km resolution (Campbell et al. 1991). For a given pair of sensors, the monthly products were first reduced to include only those bins where both sensors had valid retrievals, to ensure equivalency of spatial sampling. These common bins were then further restricted to include only those bins where water-depth is greater than 1000 meters, and an average was computed over this geographic subset for each month of the timeseries. Other geographic subsets assessed in Tables 6 and 7 include regions at different mean chlorophyll ranges, as defined by the SeaWiFS mission mean retrievals in each bin, which serve as a proxy for different trophic regions of the oceans. These include oligotrophic (Chl a < 0.1), mesotrophic (0.1 < Chl a < 1), and eutrophic (1 < Chl a < 10) bin subsets.

Figure 3a shows a comparison of global mean deep-water $R_{rs}(\lambda)$ trends for MODISA and SeaWiFS, and Figure 3b shows the ratio of MODISA to SeaWiFS $R_{rs}(\lambda)$ for the closest band centers. Statistical analysis of the two sets of trends is provided in Table 6. The results show good agreement where the spectral band centers are the same or very similar. At the common band center wavelengths of 412 and 443 nm, for example, Table 6 shows that the median ratio and mean APD agree to 1% or better when averaged over the common mission lifespan, and the mean R_{rs} retrievals agree to within 5% at all times. Agreement in deep-water Chl *a* timeseries between SeaWiFS and MODISA (Figures 3c and 3d) is also quite good, with mean ratios within 10% over all months and within 3% on average, and median APD within 3%. When restricted to oligotrophic waters (Table 6), agreement in $R_{rs}(\lambda)$ and Chl *a* between the two sensors is as good or better, which may be reflective of the fact that both sensors are absolutely calibrated to the MOBY buoy that is located in the oligotrophic waters south of Lanai, Hawaii, but agreement does not significantly degrade in the slightly more complex mesotrophic waters, which is likely reflective of the fact that non- or weakly-absorbing marine aerosols dominate these open-ocean waters, and these common marine aerosols are well handled by the atmospheric correction process. In the largely coastal eutrophic waters, however, MODISA Chl *a* retrievals are biased high relative to SeaWiFS by 18% on average, with a mean APD of 16%. This may be due in part to differences in the chlorophyll algorithm tuning that must compensate for the fact that MODISA does not have the 510-nm band, which is active in the SeaWiFS algorithm in these higher chlorophyll waters, but atmospheric correction errors or uncorrected out-of-band response likely play a significant role as well.

Agreement in the MODIST $R_{rs}(\lambda)$ timeseries relative to SeaWiFS, as provided in Figure 4 and Table 7, is similar to and in some wavelengths actually better than that of MODISA relative to SeaWiFS, but MODIST was temporally calibrated to SeaWiFS in the R2010.0 reprocessing, so good temporal correlation is to be expected. Notably, the MODIST Chl *a* retrievals are biased low by 5-10% relative to SeaWiFS in all trophic levels, including the eutrophic, yet MODIST uses exactly the same Chl *a* algorithm as MODISA.

CONCLUSIONS

The SeaWiFS mission is the first decadal scale climate data record for ocean chlorophyll and, by proxy, phytoplankton biomass, and has provided the research community with a wealth of new knowledge on ocean ecosystem and carbon cycle dynamics. The instrument temporal calibration is very well characterized (Eplee et al. 2013), and the vicariously calibrated instrument and atmospheric

correction of R2010.0 has been shown to produce $R_{rs}(\lambda)$ and Chl *a* retrievals that are in good agreement with field measurements. Using a common calibration and processing approach, MODISA R2012.0 $R_{rs}(\lambda)$ and Chl *a* retrievals have been shown to be in very good agreement with SeaWiFS retrievals over most of the world's oceans (with some significant bias in complex coastal regions). This agreement is a critical achievement for ocean biogeochemical research, as it suggests that MODISA can be used to extend the continuous ocean color time-series that started in 1997 and ended with the demise of SeaWiFS in 2010. This is illustrated in Figure 7, which shows the Chl *a* monthly timeseries for oligotrophic, mesotrophic, and eutrophic waters, as indendently derived from the SeaWiFS, MODISA, and MODIST missions. The absolute and temporal consistency over the common mission lifespan of SeaWiFS and MODISA for both oligotrophic and mesotrophic waters strongly suggests that the combined mission datasets, after reprocessing with common calibration methods and algorithms, can provide a continuous record of phytoplankton biomass for the global oceans now extending nearly 15 years.

The quality and consistency of the MODIST timeseries is degraded relative to MODISA and SeaWiFS, especially after 2010 where the loss of SeaWiFS as a stable calibration source has also resulted in a loss of temporal calibration and polarization characterization knowledge for MODIST. A reprocessing of MODIST is anticipated in the near future, using the MCST desert-based approach for temporal calibration, in hopes of further improving the quality of the MODIST timeseries.

ACKNOWLEDGEMENTS

We wish to thank all those who have collected and contributed field data to the SeaBASS archive. We also thank Giuseppe Zibordi and the AERONET-OC support team and data contributors, as well as the entire Ocean Biology Processing Group at NASA for all their many contributions to this work, with special thanks to Chris Proctor and Jason Lefler for generating the in situ match-up statistics and plots that are now available through the SeaBASS portal (http://seabass.gsfc.nasa.gov/).

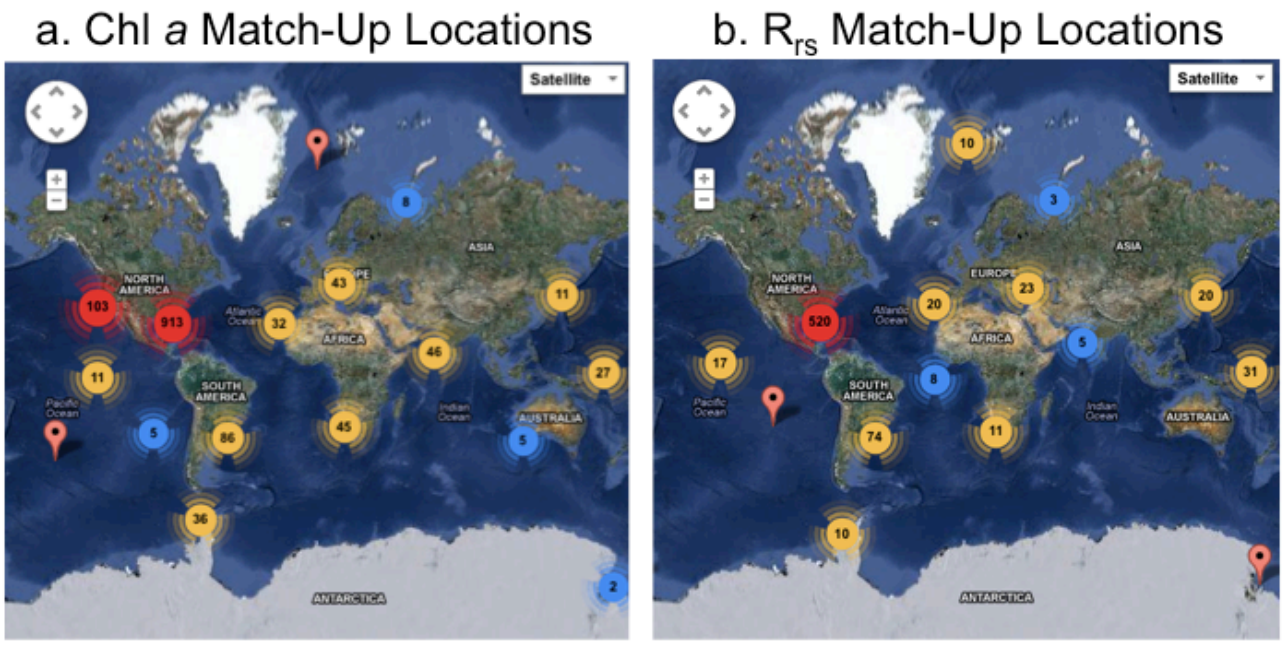

Figure 1: *Geographic distribution of SeaWiFS match-ups with SeaBASS and AERONET-OC in situ archives. Numbers indicate number of unique locations within a clustered region, with colors to emphasize higher numbers in red, lower numbers in blue. Note that match-up locations for Chl a and R_{rs} may differ, as not all field programs collect both water constituent data and radiometry.*

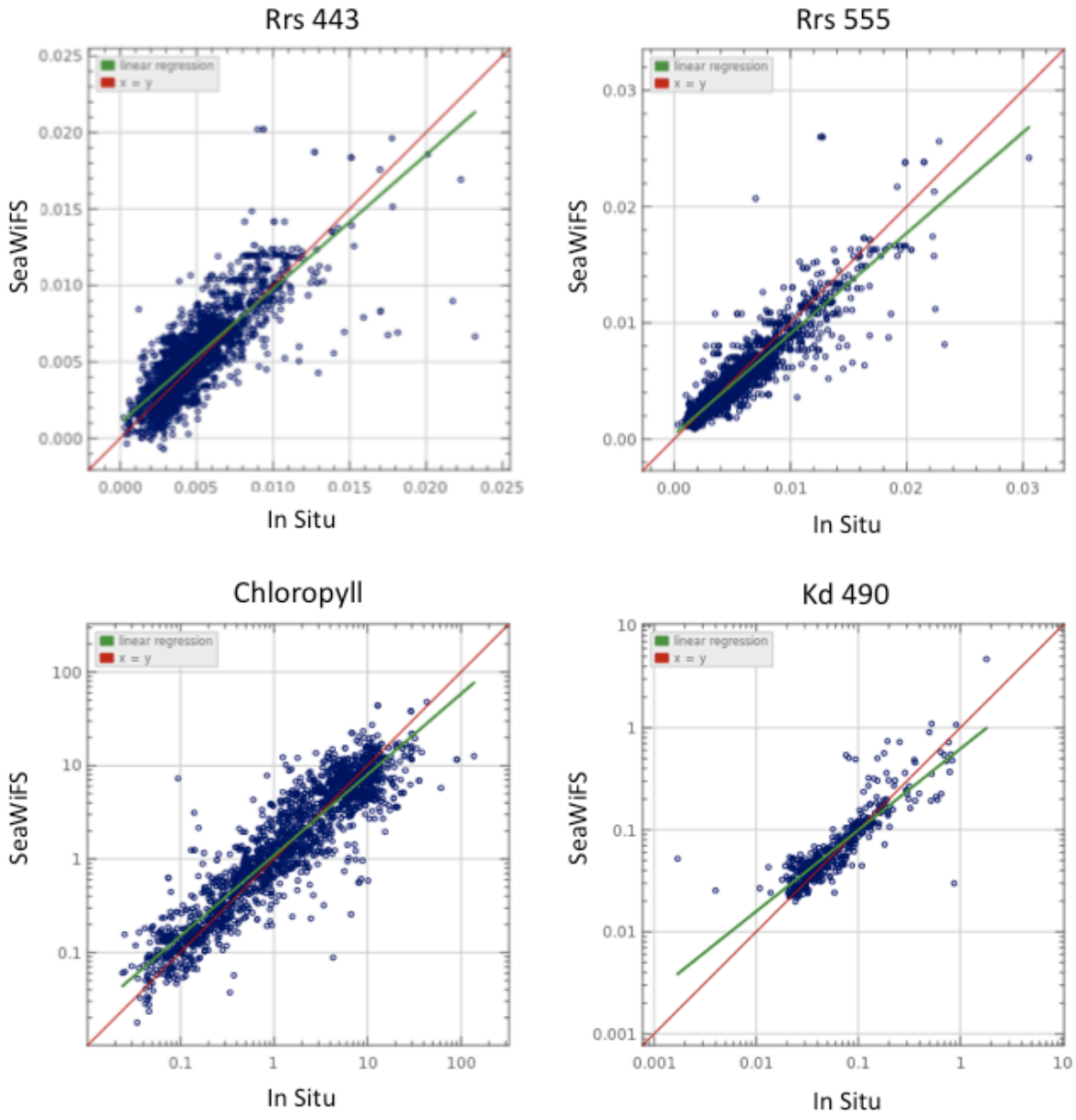

Figure 2: *Comparison of SeaWiFS-retrieved Chl a, Kd490, and R_{rs} with SeaBASS and AERONET-OC in situ archives.*

B.A. Franz, S.W. Bailey, G. Meister, and P.J. Werdell, "Consistency of the NASA Ocean Color Data Record," *Proc. Ocean Optics 2012*, Glasgow, Scotland, 8-12 October 2012.

Sensor	Product	Number of Points			R^2			Median Ratio			Mean APD		
		aeronet	seabss	deep	aeronet	seabss	deep	aeronet	seabss	deep	aeronet	seabss	deep
SeaWiFS	Rrs 412	2195	717	242	0.52	0.66	0.84	1.10	0.90	1.01	25.41	23.66	15.45
MODISA	Rrs 412	1893	244	115	0.61	0.69	0.88	0.83	0.88	0.98	35.15	23.09	10.06
MODIST	Rrs 412	5064	407	137	0.57	0.72	0.83	1.09	0.85	1.00	42.36	26.15	13.69
SeaWiFS	Rrs 443	2021	948	415	0.68	0.68	0.80	1.14	0.97	1.01	20.63	17.09	13.34
MODISA	Rrs 443	941	398	255	0.84	0.73	0.76	1.02	0.99	1.04	15.81	14.97	11.24
MODIST	Rrs 443	3677	625	313	0.81	0.72	0.71	1.10	0.93	1.01	21.42	18.07	15.22
SeaWiFS	Rrs 490	2195	969	424	0.82	0.73	0.66	0.95	0.94	0.97	11.29	14.48	11.48
MODISA	Rrs 488	1893	416	270	0.88	0.83	0.64	0.86	0.94	0.97	16.83	10.61	8.06
MODIST	Rrs 488	5064	642	322	0.91	0.79	0.58	0.93	0.93	0.98	12.68	13.07	11.02
SeaWiFS	Rrs 510	0	776	312		0.78	0.25		0.93	0.96		14.61	12.29
MODISA	Rrs 531	515	64	13	0.83	0.91	0.48	0.83	0.93	0.93	18.79	9.52	8.28
MODIST	Rrs 531	1022	130	22	0.87	0.87	0.46	0.90	1.00	1.01	12.43	13.06	8.84
SeaWiFS	Rrs 555	2141	709	242	0.82	0.84	0.40	0.94	0.93	0.98	11.29	17.08	13.63
MODISA	Rrs 547	53	44	0	0.73	0.89		0.88	0.94		16.53	12.47	
MODIST	Rrs 547	486	94	3	0.84	0.85	0.65	0.88	1.00	1.05	14.34	11.85	7.64
SeaWiFS	Rrs 670	72	458	90	0.57	0.83	0.30	0.88	0.91	1.31	24.54	36.53	53.11
MODISA	Rrs 667	0	303	227		0.93	0.03		0.94	1.00		31.86	33.47
MODIST	Rrs 667	0	406	245		0.85	0.03		0.76	0.79		39.51	44.67

Table 3: *Statistical Comparison of $R_{rs}(\lambda)$ measurements from SeaBASS and AERONET-OC in situ datasets with satellite retrievals from SeaWiFS, MODISA, and MODIST. Also shown are results for the SeaBASS comparisons when restricted to deep-water measurements (water-depth greater than 1000 meters). Analysis includes the number of satellite to in situ match-ups, the R^2 to assess correlation, the median ratio of satellite to in situ reflectances as an indicator of mean bias, and the mean absolute percent difference as a measure of uncertainty.*

Sensor	Product	Number of Points		R^2		Median Ratio		Mean APD	
		seabss	deep	seabss	deep	seabss	deep	seabss	deep
SeaWIFS	Chl *a*	1968	361	0.85	0.69	1.06	1.00	36.23	30.29
MODISA	Chl *a*	624	85	0.85	0.86	1.15	0.96	34.98	24.44
MODIST	Chl *a*	1285	178	0.78	0.67	1.01	0.94	37.81	28.30
SeaWiFS	Kd 490	463	302	0.75	0.50	1.07	1.09	18.51	19.36
MODISA	Kd 490	261	225	0.71	0.63	1.10	1.08	19.45	19.11
MODIST	Kd 490	330	241	0.78	0.66	1.03	1.05	19.86	20.61

Table 4: *Statistical Comparison of Chl a and Kd490 measurements from the SeaBASS in situ datasets with satellite retrievals from SeaWiFS, MODISA, and MODIST. Also shown are results when restricted to deep-water measurements (water-depth greater than 1000 meters). Analysis includes the number of satellite to in situ match-ups, the R^2 to assess correlation, the median ratio of satellite to in situ reflectances as an indicator of bias, and the mean absolute percent difference as a measure of uncertainty.*

Sensors	Product	Number of Points	R^2	Median Ratio	Mean APD
SeaWiFS & MODISA	Rrs 412	1265	0.79	0.84	22.94
SeaWiFS & MODIST	Rrs 412	2078	0.75	0.98	23.66
SeaWiFS & MODISA	Rrs 443	1265	0.88	0.91	13.64
SeaWiFS & MODIST	Rrs 443	2078	0.85	0.98	13.16
SeaWiFS & MODISA	Rrs 490 & 488	1265	0.94	0.97	8.20
SeaWiFS & MODIST	Rrs 490 & 488	2078	0.92	1.01	8.39
SeaWiFS & MODISA	Rrs 510 & 531	1265	0.92	0.98	10.65
SeaWiFS & MODIST	Rrs 510& 531	2078	0.90	0.99	10.49
SeaWiFS & MODISA	Rrs 555 & 547	1265	0.95	1.02	8.94
SeaWiFS & MODIST	Rrs 555 & 547	2078	0.93	1.03	9.44
SeaWiFS & MODISA	Rrs 670 & 667	1265	0.92	0.93	19.50
SeaWiFS & MODIST	Rrs 670 & 667	2078	0.85	0.82	28.60
SeaWiFS & MODISA	Chl *a*	1265	0.93	1.05	12.52
SeaWiFS & MODIST	Chl *a*	2078	0.93	0.97	12.36
SeaWiFS & MODISA	Kd 490	1265	0.91	1.02	7.64
SeaWiFS & MODIST	Kd 490	2078	0.89	0.97	7.80

Table 5: *Statistical comparison of Rrs(λ), Chl a, and Kd490 satellite retrievals at common match-up locations between SeaWiFS and MODISA, and between SeaWiFS and MODIST. Analysis includes the number of satellite to satellite match-ups, the R^2 to assess correlation, the median ratio of satellite to satellite reflectances as an indicator of bias, and the mean absolute percent difference as a measure of uncertainty.*

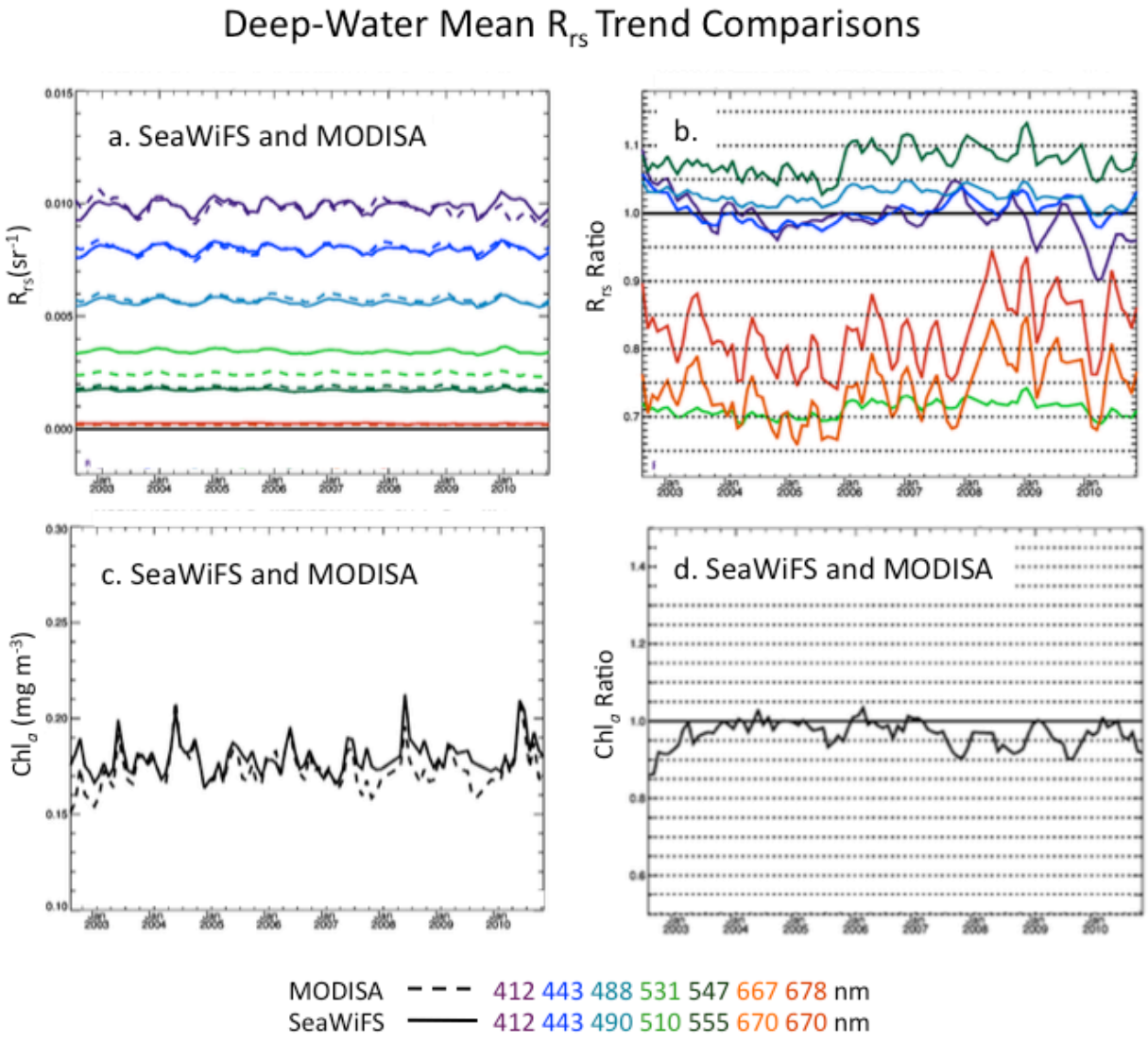

Figure 3: *Comparison of MODISA ocean color time-series with SeaWiFS, and ratio of MODISA to SeaWiFS, for spectral remote sensing reflectance and chlorophyll over the common mission lifespans. Trends were derived from monthly Level-3 binned products, reduced to common bins, and averaged to over all bins where water depth is greater than 1000 meters.*

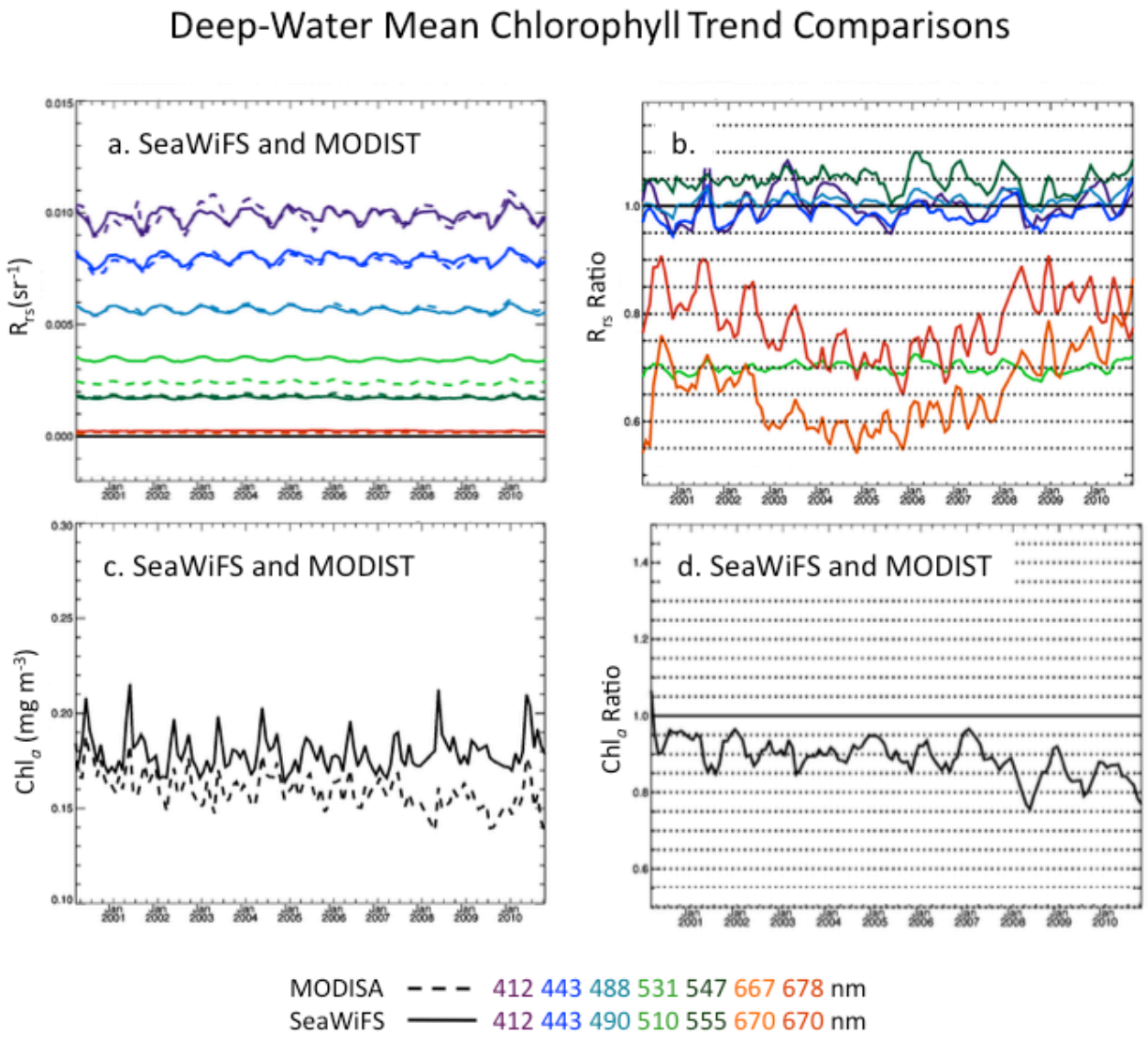

Figure 4: *Comparison of MODIST ocean color time-series with SeaWiFS, and ratio of MODIST to SeaWiFS, for spectral remote sensing reflectance and chlorophyll over the common mission lifespans. Trends were derived from monthly Level-3 binned products, reduced to common bins, and averaged to over all bins where water depth is greater than 1000 meters.*

B.A. Franz, S.W. Bailey, G. Meister, and P.J. Werdell, "Consistency of the NASA Ocean Color Data Record," *Proc. Ocean Optics 2012*, Glasgow, Scotland, 8-12 October 2012.

Region	Product	SeaWiFS Mean	MODISA Mean	Median Ratio	R^2	Mean APD
Deep	Rrs 412	0.0099	0.0099	1.00	0.60	1.07
Deep	Rrs 443	0.0080	0.0080	1.00	0.57	0.88
Deep	Rrs 490 & 488	0.0056	0.0058	1.04	0.99	3.68
Deep	Rrs 510 & 531	0.0034	0.0025	0.72	0.91	32.34
Deep	Rrs 555 & 547	0.0017	0.0019	1.10	0.82	9.13
Deep	Rrs 670 & 667	0.0003	0.0002	0.75	0.04	28.23
Deep	Rrs 670 & 678	0.0003	0.0002	0.83	0.03	18.43
Deep	Chl *a*	0.179	0.174	0.97	0.65	2.30
Olig	Rrs 412	0.0139	0.0139	1.00	0.89	0.95
Olig	Rrs 443	0.0106	0.0107	1.01	0.86	0.96
Olig	Rrs 490 & 488	0.0065	0.0069	1.06	0.82	4.99
Olig	Rrs 510 & 531	0.0035	0.0023	0.68	0.28	38.10
Olig	Rrs 555 & 547	0.0015	0.0017	1.13	0.07	11.99
Olig	Rrs 670 & 667	0.0002	0.0002	0.77	0.34	26.83
Olig	Rrs 670 & 678	0.0002	0.0002	0.79	0.40	23.42
Olig	Chl *a*	0.060	0.058	0.96	0.79	5.42
Meso	Rrs 412	0.0075	0.0075	0.99	0.61	1.85
Meso	Rrs 443	0.0065	0.0064	0.99	0.70	1.83
Meso	Rrs 490 & 488	0.0051	0.0053	1.03	0.99	2.70
Meso	Rrs 510 & 531	0.0034	0.0026	0.75	0.95	28.46
Meso	Rrs 555 & 547	0.0018	0.0020	1.08	0.92	8.05
Meso	Rrs 670 & 667	0.0003	0.0002	0.74	0.00	29.47
Meso	Rrs 670 & 678	0.0003	0.0002	0.84	0.01	17.26
Meso	Chl *a*	0.252	0.244	0.97	0.71	2.39
Eutr	Rrs 412	0.0030	0.0028	0.94	0.59	9.85
Eutr	Rrs 443	0.0037	0.0035	0.95	0.85	5.21
Eutr	Rrs 490 & 488	0.0043	0.0043	1.00	1.00	0.42
Eutr	Rrs 510 & 531	0.0043	0.0043	1.00	0.99	1.45
Eutr	Rrs 555 & 547	0.0041	0.0041	1.00	1.00	0.71
Eutr	Rrs 670 & 667	0.0011	0.0010	0.91	1.00	9.35
Eutr	Rrs 670 & 678	0.0011	0.0010	0.95	1.00	4.36
Eutr	Chl *a*	2.091	2.468	1.18	0.71	16.23

Table 6: *Statistical comparison of global Rrs(λ), Chl a, and Kd490 satellite retrievals for the common mission lifespans of SeaWiFS and MODISA. Results were derived from global Level-3 monthly binned products, and statistics were derived for four different global geographic subsets, including global deep water (all bins where depth is greater than 1000-meter), and global oligotrophic, mesotrophic, and eutrophic waters as defined by typical Chl a ranges (Chl a < 0.1, 0.1 < Chl a < 1.0, and Chla > 1.0 mg m^{-3}, respectively). Analysis includes the mean values, the R^2 to assess correlation, the median ratio of satellite to satellite reflectances as an indicator of bias, and the mean absolute percent difference as a measure of uncertainty.*

Region	Product	SeaWiFS Mean	MODIST Mean	Median Ratio	R^2	Mean APD
Deep	Rrs 412	0.0099	0.0099	1.00	0.51	1.84
Deep	Rrs 443	0.0080	0.0079	0.99	0.69	1.68
Deep	Rrs 490 & 488	0.0057	0.0057	1.01	0.83	1.14
Deep	Rrs 510 & 531	0.0035	0.0024	0.70	0.80	35.76
Deep	Rrs 555 & 547	0.0018	0.0018	1.04	0.51	4.08
Deep	Rrs 670 & 667	0.0003	0.0002	0.58	0.16	53.28
Deep	Rrs 670 & 678	0.0003	0.0002	0.70	0.08	34.71
Deep	Chl *a*	0.178	0.159	0.89	0.34	11.14
Olig	Rrs 412	0.0138	0.0138	1.00	0.80	1.77
Olig	Rrs 443	0.0106	0.0105	0.99	0.86	1.35
Olig	Rrs 490 & 488	0.0065	0.0067	1.02	0.67	1.99
Olig	Rrs 510 & 531	0.0035	0.0023	0.65	0.45	42.16
Olig	Rrs 555 & 547	0.0016	0.0017	1.07	0.25	5.59
Olig	Rrs 670 & 667	0.0002	0.0001	0.59	0.56	52.51
Olig	Rrs 670 & 678	0.0002	0.0002	0.66	0.50	41.85
Olig	Chl *a*	0.061	0.057	0.94	0.81	5.83
Meso	Rrs 412	0.0076	0.0076	1.01	0.54	2.30
Meso	Rrs 443	0.0065	0.0064	0.99	0.74	1.61
Meso	Rrs 490 & 488	0.0052	0.0052	1.00	0.90	0.70
Meso	Rrs 510 & 531	0.0035	0.0025	0.73	0.91	31.34
Meso	Rrs 555 & 547	0.0019	0.0020	1.03	0.74	3.04
Meso	Rrs 670 & 667	0.0003	0.0002	0.59	0.03	52.44
Meso	Rrs 670 & 678	0.0003	0.0002	0.73	0.00	32.38
Meso	Chl *a*	0.250	0.221	0.89	0.41	11.93
Eutr	Rrs 412	0.0030	0.0032	1.09	0.68	8.50
Eutr	Rrs 443	0.0037	0.0037	1.00	0.93	2.48
Eutr	Rrs 490 & 488	0.0044	0.0044	1.01	0.98	1.21
Eutr	Rrs 510 & 531	0.0043	0.0042	0.98	0.98	3.42
Eutr	Rrs 555 & 547	0.0041	0.0039	0.97	1.00	3.00
Eutr	Rrs 670 & 667	0.0011	0.0009	0.87	0.99	15.45
Eutr	Rrs 670 & 678	0.0011	0.0010	0.92	0.99	9.68
Eutr	Chl *a*	2.090	1.940	0.93	0.53	7.66

Table 7: *Statistical comparison of global Rrs(λ), Chl a, and Kd490 satellite retrievals for the common mission lifespans of SeaWiFS and MODIST. Results were derived from global Level-3 monthly binned products, and statistics were derived for four different global geographic subsets, including global deep water (all bins where depth is greater than 1000-meter), and global oligotrophic, mesotrophic, and eutrophic waters as defined by typical Chl a ranges (Chl a < 0.1, 0.1 < Chl a < 1.0, and Chla > 1.0 mg m^{-3}, respectively). Analysis includes the mean values, the R^2 to assess correlation, the median ratio of satellite to satellite reflectances as an indicator of bias, and the mean absolute percent difference as a measure of uncertainty.*

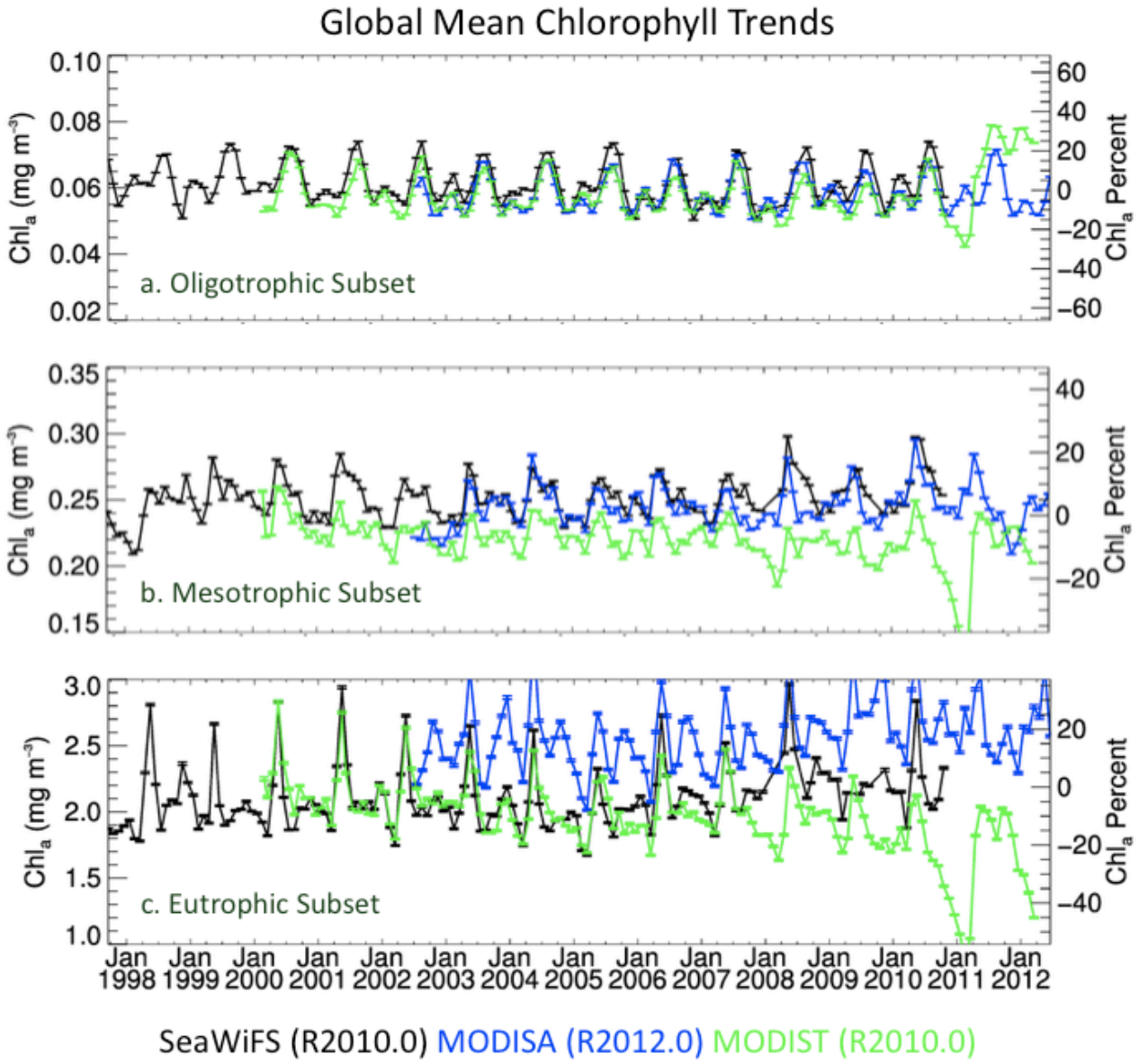

Figure 5: *Chlorophyll timeseries derived independently from SeaWiFS, MODISA, and MODIST. Trends were derived from monthly Level-3 binned products, reduced to common bins, and averaged over all bins were water is characterized as typically a) oligotrophic, b) mesotrophic, and c) eutrophic.*

REFERENCES

Ahmad, Z., B.A. Franz, C.R. McClain, E.J. Kwiatkowska, J. Werdell, E.P. Shettle, and B.N. Holben (2010). New aerosol models for the retrieval of aerosol optical thickness and normalized water-leaving radiances from the SeaWiFS and MODIS sensors over coastal regions and Open Oceans, Appl. Opt., 49(29).

Bailey, S. W. and P. J. Werdell (2006). A multi-sensor approach for the on-orbit validation of ocean color satellite data products, Remote Sens. Environ. 102, 12--23.

Bailey, S.W., B.A. Franz and P.J. Werdell (2010). Estimation of near-infrared water-leaving reflectance for satellite ocean color data processing. *Optics Express, 18,* 7521-7527.

Behrenfeld, M.J., R.O'Malley, D.Siegel, C. McClain, J. Sarmiento, G. Feldman, A. Milligan, P. Falkowski, R. Letelier, E. Boss. (2006). Climate-driven trends in contemporary ocean productivity, Nature 444, 752-755.

Campbell, J.W., J.M. Blaisdell, and M. Darzi (1995). Level-3 SeaWiFS Data Products: Spatial and Temporal Binning Algorithms. NASA Tech. Memo. 104566, Vol. 32, S.B. Hooker, E.R. Firestone, and J.G. Acker, Eds., NASA Goddard Space Flight Center, Greenbelt, Maryland.

Chisholm, S.W. (2000). Stirring times in the Southern Ocean. Nature 407:685-686, 12 October 2000.

Clark, D. K., H. R. Gordon, K. J. Voss, Y. Ge, W. W. Broenkow, and C. Trees (1997). Validation of atmospheric correction over the oceans, J. Geo. Res. 102, 17209– 17217.

Eplee, R.E., Jr., G. Meister, F.S. Patt, S.W. Bailey, and C.R. McClain (2012). The On-Orbit Calibration of SeaWiFS, *submitted to Applied Optics.*

Esaias, W.E., Abbott, M.R., Barton, I., Brown, O.B., Campbell, J.W., Carder, K.L., Clark, D.K., Evans, R.H., Hoge, F.E., Gordon, H.R., Balch, W.M., Letelier, R., and Minnett, P.J. (1998), An overview of MODIS capabilities for ocean science observations. *IEEE Transactions on Geoscience and Remote Sensing*, 36, 1250-1265.

Franz, B.A., R.E. Eplee, Jr., S.W. Bailey, and M. Wang (2003), Changes to the atmospheric correction algorithm and retrieval of oceanic optical properties. NASA/TM-2003-206892, Vol. 22, NASA Goddard Space Flight Center, Greenbelt, Maryland, 29-33.

Franz, B.A., S.W. Bailey, P.J. Werdell, and C.R. McClain, F.S. (2007). Sensor-independent approach to vicarious calibration of satellite ocean color radiometry, Appl. Opt., 46 (22).

Franz, B.A., E.J. Kwiatkowska, G. Meister, and C. McClain (2008). Moderate Resolution Imaging Spectroradiometer on Terra: limitations for ocean color applications, J. Appl. Rem. Sens., 2, 023525.

Gordon, H.R., and Wang, M. (1994), Retrieval of water-leaving radiance and aerosol optical-thickness over the oceans with SeaWiFS – a preliminary algorithm. *Applied Optics*, 33, 443-452.

Gordon H.R. (1995), Remote sensing of ocean color: A methodology for dealing with broad spectral bands and significant out-of-band response. *Applied Optics*, 34: (36) 8363-8374.

Kwiatkowska, E.J., B.A. Franz, G. Meister, C. McClain, and X. Xiong (2008). Cross-calibration of ocean-color bands from Moderate Resolution Imaging Spectroradiometer on Terra platform, Appl. Opt., 47 (36).

McClain CR, Cleave ML, Feldman GC, et al. (1998). Science quality SeaWiFS data for global biosphere research, *Sea Technol* 39: (9) 10-16.

Meister, G., Kwiatkowska, E., Franz, B.A., Patt, F.S., Feldman, G.C., McClain, C.R. (2005), The MODIS ocean color polarization correction, Appl. Opt., 44 (26) 5524-5535.

Meister. G., B.A. Franz, E.J. Kwiatkowska, and C. R. McClain (2012). Corrections to the Calibration of MODIS Aqua Ocean Color Bands Derived From SeaWiFS Data, T. Geo. Rem. Sens., 50 (1).

Meister. G., B.A. Franz, and C. R. McClain (2013). Corrections to the Calibration of MODIS Aqua Ocean Color Bands Derived From MODIS Aqua Level 3 data, in preparation.

Morel, A., and L. Prieur (1977). Analysis of variations in ocean color, Limnology and Oceanography 22, 709e722.

National Research Council (2004). Climate data records from environmental satellites, National Academy Press, Washington, DC, 150 pp.

OBPG (2012a). l2gen: The Multi-Sensor Level-1 to Level-2 Generator, Ocean Color Web, http://oceancolor.gsfc.nasa.gov/WIKI/OCSSW(2f)l2gen.html.

OBPG (2012b). Ocean Color Chlorophyll (OC) v6. http://oceancolor.gsfc.nasa.gov/REPROCESSING/R2009/ocv6/

OBPG (2012c). Diffuse attenuation coefficient (KD) for downwelling irradiance at 490-nm. http://oceancolor.gsfc.nasa.gov/REPROCESSING/R2009/ocv6/

Siegel, D.A. and B.A. Franz (2010). Century of phytoplankton change, Nature, 466, 569-571, doi:10.1038/466569.a

Thuillier, G., M. Hersé, P. C. Simon, D. Labs, H. Mandel, D. Gillotay, and T. Foujols (2003). The solar spectral irradiance from 200 to 2400 nm as measured by the SOLSPEC spectrometer from the ATLAS 1-2-3 and EURECA missions, Solar Physics, 214(1): 1-22.

Wang, M., Franz, B.A., Barnes, R.A., and McClain, C.R. (2001). Effects of spectral bandpass on SeaWiFS-retrieved near-surface optical properties of the ocean. *Applied Optics*, 40: 343-348.

Wang, M., and Sean W. Bailey, "Correction of Sun glint Contamination on the SeaWiFS Ocean and Atmosphere Products," Appl. Opt. 40, 4790-4798 (2001).

Werdell, P.J., Bailey, S., Fargion, G., Pietras, C., Knobelspiesse, K., Feldman, G., and McClain, C. (2003), Unique data repository facilitates ocean color satellite validation. *EOS Transactions AGU*, 84, 38, 379.

Werdell, P.J. and Bailey, S.W. (2005). An improved in situ bio-optical data set for ocean color algorithm development and satellite data product validation, Rem. Sens. Env., 98, 122-140.

Werdell, P.J., S.W. Bailey, B.A. Franz, A. Morel, and C.R. McClain (2007). On-orbit vicarious calibration of ocean color sensors using an ocean surface reflectance model. Appl. Opt. 46, 5649-5666.

Xiong, X., Chiang, K., Esposito, J., Guether, B., Barnes, W. (2003). MODIS on-orbit calibration and characterization, *J. Meteorologica*, 40 (2003) S89-S93.

Zibordi, G., B. Holben, S. B. Hooker, F. Melin, J.-F. Berthon, I. Slutsker, D. Giles, D. Vandemark, H. Feng, K. Rutledge, G. Schuster and A. Al Mandoos (2006). A network for standardized ocean color validation measurements. EOS Transactions American Geophysical Union, Volume 87, Issue 30, p. 293-297.